

RESEARCH ARTICLE

Pinus-derived membrane vesicles disrupt pathogenic metabolism in fungi

S. Kunene^{1,2} , T. J. Mmushi² , E. Steenkamp²  & T. Motaung² 

1 Department of Plant and Soil Science, University of Pretoria, Private Bag X20, Hatfield, 0028, South Africa

2 Department of Biochemistry, Genetics and Microbiology, and Forestry and Agricultural Biotechnology Institute, University of Pretoria, Private Bag X20, Hatfield, 0028, Pretoria, South Africa

Keywords

Biocontrol agents; filamentous pathogens; needle-derived vesicles (ndMVs); pine pitch canker disease; *Pinus* species; vesicles (Vs).

Correspondence

T. Motaung, Department of Biochemistry, Genetics and Microbiology, and Forestry and Agricultural Biotechnology Institute, University of Pretoria, Private Bag X20, Hatfield 0028, Pretoria, South Africa.

E-mail: thabiso.motaung@up.ac.za

Editor

V. Grbic

Received: 23 November 2024;

Accepted: 11 June 2025

doi:10.1111/plb.70069

ABSTRACT

- Much of what we know about the biological impacts of vesicles (MVs) is derived from *Arabidopsis thaliana*. Our study focused on vesicles from species in the non-model plant group, *Pinus* (pine) (*P. elliottii*, *P. radiata*, and *P. patula* × *Pinus tec* (hybrid)). These plants have tougher tissues and strong, acicular-shaped leaves (needles).
- Herein, we first developed a protocol to guide effective collection of juice fluid from needles and roots in a clean and efficient manner. The effects of these vesicles were characterized in terms of the global nutrient profile of the pine pitch canker fungus, *Fusarium circinatum*, generated from growing fungal spores on ~400 substrates embedded across BioLog phenotypic microarray (PM) plates (PM1, PM2A: carbon sources; PM3B: nitrogen sources; PM9: osmolytes/pH; PM24C: chemicals).
- Our findings revealed that MVs, specifically needle-derived MVs (ndMVs) from *P. elliottii*, disrupt metabolite assimilation in several important pathways, including carbon and nitrogen metabolism. The PM data were also strongly correlated with observed phenotypic effects, including reduced viability and germination of spores in liquid media, as well as impaired filamentous growth on solid media. Importantly, these MV-induced phenotypic effects were reproducible in other filamentous pathogens (e.g., *Botrytis cinerea*, *Chrysosporthe cubensis* and *F. graminearum*) and during a glasshouse trial conducted with *F. circinatum*-infected *P. elliottii* seedlings, demonstrating the stable biological effects of ndMVs.
- Cumulatively, our results suggest that plant-derived vesicles can disrupt metabolism in pathogenic fungi and, therefore, serve as a cost-effective and sustainable source of novel plant protection molecules.

INTRODUCTION

Extracellular vesicles (EVs) are membranous nanoparticles released by eukaryotes and prokaryotes, and play an important role in cross-kingdom communication. EVs have received much attention in recent years, especially in plant–pathogen interactions, where plant-derived EVs are increasingly investigated for their role in defence against pathogen attack (Rutter & Innes 2017; Cai *et al.* 2018; De Palma *et al.* 2020).

To some extent, the outcome of plant–pathogen interactions depends on vesicles secreted by both the plant and the pathogen. However, studies pertaining to vesicles from species of pine (*Pinus*) are currently unavailable, although research on other plants suggests that EVs can deliver defence-related compounds directly into pathogen cells, disrupting their cellular processes. For instance, plant vesicles are known to carry small RNAs, enzymes, and antimicrobial agents that specifically target fungal metabolic pathways, weakening the pathogen's ability to thrive within host tissues (Regente *et al.* 2017; Cai *et al.* 2018). Therefore, plant vesicles have emerged as key players in plant defence, particularly in disrupting the metabolism of fungal pathogens.

The International Society for Extracellular vesicles (ISEV) has proposed a set of “minimal experimental requirements for the definition of vesicles” (Welsh *et al.* 2024). However, the isolation of vesicles and methods used for their characterization are continuously being developed and refined, prompting ISEV to update its recommendations to allow standardized and rigorous analysis of vesicles. Consequently, many methods have been developed to extract and characterize EVs derived from plants. Among these, differential ultracentrifugation (dUC) is widely used (Gardiner *et al.* 2016), although it has been shown to have several disadvantages, including low specificity, as it may co-isolate EVs with other particles such as protein aggregates, cellular debris, and lipoproteins (Böing *et al.* 2014).

Size-exclusion chromatography (SEC) is increasingly used as an alternative, especially because it is fast and easy to set up while also allowing vesicle isolation from complex samples (Böing *et al.* 2014). Although multiple fractionation steps are often required (Böing *et al.* 2014), SEC allows for removal of most of the excess soluble plasma proteins (Gámez-Valero *et al.* 2016). SEC-based isolation also has a limited impact on the intrinsic properties of vesicles, vesicular structure and content (Böing *et al.* 2014; Gámez-Valero *et al.* 2016). In this

study, we developed a SEC-based method for the isolation of vesicles from *Pinus* species.

Pines are conifers native to the Northern Hemisphere, with a few species also in certain regions of the Southern Hemisphere (Badik *et al.* 2018). They provide various ecosystem services, while species such as *P. patula*, *P. radiata*, and *P. elliottii* are deployed in plantation forestry to meet local and global needs for wood and fibre (Morris 2022). The health of these plants is threatened by numerous pathogens (e.g., *Fusarium circinatum*, *Gymnosporangium* spp., *Bursaphelenchus xylophilus*, and *Dothistroma septosporum*; Hansen *et al.* 2018), many of which are the subject of ongoing research into mitigating disease impacts. These existing efforts to unravel *Pinus*–pathogen interactions would thus benefit from adding a vesicle dimension to the molecular processes involved.

One of the primary aims of this study was, therefore, to establish an isolation method for vesicles from the roots and needles of *Pinus* species. By modifying previously published methods, we processed samples from a homogenate (ground tissue), resulting in a mixture of intracellular and extracellular vesicles. Hence, we collectively refer to all vesicles used in this study as ‘membrane vesicles’ (MVs). The second aim was to analyse pure MVs for their bioactivity against growth of *F. circinatum*, a worrisome pathogen of pine trees that can exist in two states, namely, free-living mycelia (planktonic) and mycelia embedded in an extracellular matrix (ECM), or the biofilm state (Ratsoma *et al.* 2024). To achieve this goal, we performed assays to determine how pine needle and root-derived vesicles affect the planktonic (ECM-free) and biofilm states of *F. circinatum*; the results of which suggest that MVs prevents pathogen growth by inhibiting key metabolic and structural pathways, most of which are essential for virulence. These vesicles also maintained pine seedling health and remained effective against *F. circinatum* field isolates and other key economic filamentous pathogens, including *Botrytis cinerea*, *Chrysosporthe cubensis*, and non-*circinatum* *Fusarium* spp. Therefore, exogenous *Pinus* vesicles are potential vectors for antifungal activity as they interfere with pathogenic cellular processes.

MATERIAL AND METHODS

Plant material, fungal isolates and growth conditions

Three *Pinus* species (*P. elliottii*, *P. radiata*, and *P. patula* × *P. tec* (hybrid)) were used, with 3-month-old seedlings obtained from the Karatara nursery in Western Cape Province, South Africa. These seedlings were maintained in a controlled environment at the phytotron of the Forestry and Agricultural Biotechnology Institute (FABI), University of Pretoria, South Africa. The seedlings were exposed to natural sunlight through the glass panels of the glasshouse, without any artificial lighting. Temperature and humidity levels in the phytotron ranged from 14.1°C to 33°C and from 11% to 99%, respectively, with these fluctuations occurring on a daily basis. Growth was assessed on a peat-based substrate, which was watered three times a week and monitored over time. We obtained the fungal isolates (Table S1) from the *Fusarium* collection located at FABI, University of Pretoria, South Africa. The isolates were routinely cultured on quarter potato dextrose agar (PDA) (Merck) then incubated at 25°C in the dark for 7 days prior to downstream analysis.

Table 1. List of fungal isolates selected for screening response to *Pinus*-derived membrane vesicles.

Pathogen	Strain
<i>Fusarium circinatum</i> (FSP34)	CMWF350
<i>Fusarium circinatum</i>	CMWF2654
<i>Fusarium circinatum</i>	CMWF5689
<i>Fusarium circinatum</i>	CMWF2552
<i>Botrytis cinerea</i>	CMW13135
<i>Chrysosporthe cubensis</i>	CMW54409
<i>Fusarium graminearum</i>	CMW58100
<i>Fusarium graminearum</i>	CMW58100
<i>Fusarium verticillioides</i>	CMW59120
<i>Fusarium circinatum</i>	CMWF2652

Preparation and purification of pine-derived vesicles

Crude extracts were prepared from needles and roots of 3-month-old pine seedlings by grinding plant material in a vesicle isolation buffer, followed by differential centrifugation and filtration to obtain the juice fluid (JF) (see Supplementary Information S1). Vesicles were subsequently purified from the JF using size exclusion chromatography (SEC) on Sepharose CL-2B columns. Vesicle-containing fractions were identified by fluorescence labelling with the lipophilic dye FM4-64 and pooled for downstream analyses. Detailed protocols for sample preparation, centrifugation steps, buffer compositions, and SEC procedures are provided in the Supplementary Information (S1).

Physical characterization of pure vesicles

For transmission electron microscopy (TEM), samples obtained via SEC were prepared as described in Barreto-Vieira & Barth (2015). Briefly, a drop of sample and 3% phosphotungstic acid were mixed, and a formvar/carbon-coated grid (coated side below) placed on top of the mixture. After 30 s, the grid was removed, and excess fluid drained through a filter paper. Finally, the samples containing vesicles were visualized using TEM (JOEL JEM 2100F; JOEL, Tokyo, Japan) at three different magnifications (1500, 15 000, and 50 000). Nanoparticle tracking analysis (NTA) was performed using a NanoSight NS500 (Malvern Panalytical, Malvern, UK). All samples were ultrasonicated for 10 min before analysis and subsequently filtered using a 0.45-µm syringe filter (Merck, Johannesburg, South Africa). This was followed by particle analysis for each sample, with a 60 s video captured at camera levels ranging from 4 to 15. All the sample dilutions were performed using PBS, and the samples were then analysed in 15 technical replicates.

Investigating fungal response to pine vesicles

The impact of vesicles on fungal spore germination

To investigate the impact of vesicles on fungal spore germination in *F. circinatum* isolate (CMWF350) (Table S1), we first determined the concentrations of vesicles from pine seedling needles (ndMVs) and roots (rdMVs) for the pine species (*P. radiata*, *Pinus* hybrid, and *P. elliottii*) by assessing protein content using the QuantiPro™ BCA assay Kit (Merck), following

guidelines provided by the manufacturer. Fungal spores from the plate culture were harvested by adding 2 mL 0.2 M phosphate-buffered saline (PBS: 10 mM NaH₂PO₄, 10 mM Na₂HPO₄, and 150 mM NaCl at pH 7.2). A Countess 3 Automated Cell Counter (Thermo Fisher Scientific) was used to quantify the collected spores for use in the analyses. Subsequently, we followed established methods to explore the interaction between *F. circinatum* fungal spores and vesicles by evaluating spore viability, germination of hyphae (germ tubes), or the ability of these spores to form a fungal biofilm (Ratsoma *et al.* 2024). Briefly, fungal spores were co-incubated with vesicles at three concentrations (5, 10, and 15 µg mL⁻¹), with the control groups consisting of spores without vesicle treatment (positive control; spores + ¼ PDB). The ¼ PDB without spores served as negative control. We then performed cell counts using Countess 3 FL to determine how many spores developed hyphae (germ tubes) out of the total number of spores counted. The cells were then stained with trypan blue to determine viability. This two-step approach was used to determine how vesicles impact both the overall germination rate and cell viability, thus providing a comprehensive picture of the effect of vesicles on early growth.

The germ tubes were counted using a haemocytometer under a light microscope to determine the potential for conidia to form hyphae (germination) and biofilm communities, the results of which were recorded within 2 to 24 h of shaking (Orbital shaker, 160 rpm; Reflecta Laboratory Suppliers). We also examined samples under a light microscope within 24 and 72 h, followed by image capture directly under the microscope.

The impact of vesicles on fungal morphology

We additionally investigated how vesicles might influence the colony and cellular morphology of *F. circinatum*. To achieve this, we treated a conidial suspension (5 × 10⁵ spores mL⁻¹) with 15 µg mL⁻¹ ndMV and rdMV for 24 h. These vesicle-exposed spores were cultivated on ¼ PDB and allowed to grow for 3, 7, and 14 days in 90 × 15 mm Petri dishes containing ¼ PDA. Throughout this time, we quantified radial growth by measuring the diameter of colonies growing on ¼ PDA in three biological replicates. Additionally, we examined fungal cells under SEM; cells were carefully removed from the PDA plates using a spatula, and transferred to Eppendorf tubes containing a fixative solution (glutaraldehyde) for 30 min to preserve the cell structure. Following fixation, the cells were dehydrated in an ethanol series (30%, 50%, 70%, 90% and 100%) for 15 min each and coated with a pure platinum (Pt) metal foil to improve conductivity of the cells and reduce charging effects, which can distort images and interfere with imaging quality. SEM imaging was then performed using FEGSEM (Zeiss 540 Ultra) at 10× magnification to analyse cell morphology, size, and surface features.

The impact of vesicles on biofilm growth

Vesicles were combined with conidia as described above, but this time, the pair was incubated under non-shaking conditions to allow fungal spores to settle on an abiotic surface and begin to form a biofilm. Biofilm formation was then allowed to occur in 96-well polystyrene plates for up to 7 days, with 72 h and 7 days representing early-maturity and late-maturity biofilms, respectively. Once formed, biomass and extracellular matrix (ECM), the two most important biofilm traits, were measured according to Ratsoma *et al.* (2024). To measure these biofilm

markers, biofilms were fixed with methanol and air-dried, followed by addition of crystal violet solution, which stains biomass in both live and dead cells as well as certain components within the biofilm matrix. The suspension was incubated at room temperature for 30–60 min and washed, after which biomass absorbance was measured at 540 nm using a spectrophotometer (SpectraMax paradigm, Multimode detection platform). To assess the ECM, biofilms were subjected to basic fuchsin staining, allowing visualization and distribution of polysaccharides in the matrix. After staining, the excess dye was removed, and the stained polysaccharides quantified at 530 nm using a microplate reader, as described above. The controls included biofilms without vesicle treatment (positive control) and ¼ PDB (negative control).

Screening field isolates and non-F. Circinatum species against vesicles

The influence of vesicles on the colony and cellular morphology of another three *Fusarium circinatum* isolates (CMWF2552, CMWF2654, and CMWF5689) was conducted as described for the FSP34 isolate. Briefly, a conidial suspension was exposed to 15 µg mL⁻¹ ndMV in ¼ PDB for 24 h and allowed to grow for 3, 7, and 14 days on ¼ PDA. This was followed by quantification of radial growth in three biological replicates. Additionally, fungal cells on the plates were observed under a light microscope at 20× magnification, and images were captured directly from the microscope. The responses of 14 filamentous fungi against 15 µg mL⁻¹ and 30 µg mL⁻¹ of vesicles was similarly investigated; however, only radial growth was measured at 3, 7, and 14 days. The list of species included several important plant pathogens infecting a wide host range is provided in Table S1.

Global nutrient profiling in the presence of vesicles

Preparation of cell suspensions

The FSP34 isolate (CMWF350) was selected as the primary strain for global nutrient profiling. Fungal spores from this isolate were harvested, and concentration adjusted as described previously, followed by exposure to 15 µg mL⁻¹ vesicles. Vesicle-exposed and untreated spores were then transferred to sterile capped tubes containing 12 mL sterile FF-IF. The suspension was homogenized by stirring with a swab, avoiding turbulent mixing.

Inoculation of PM1, PM2A, PM3B, PM9 and PM24C plates

A volume of 50 µL of cell suspension was added to 23.95 mL PM1, PM2A inoculating fluid, and 100 µL of this suspension was inoculated into the PM1 and PM2A panels per well. For PM3B, 125 µL of cell suspension was added to 59.875 mL PM3B inoculating fluid, and 100 µL of this suspension was inoculated into the PM3B panels per well. A volume of 30 µL cell suspension was added to 143.7 mL PM9 and PM24C inoculation fluid, and 100 µL of this suspension was inoculated into the PM9 panels per well. For all PM panels, the plates were sealed with polyester sealing tape and incubated in a conventional mechanical incubator (BEING Scientific, USA) at 26°C for 24 h to 21 days. After incubation, the plates were removed from the incubator and stored at 4°C for 10 min. The data were collected by reading the plates using a SpectraMax M2 plate reader (MedQ) at 750 nm.

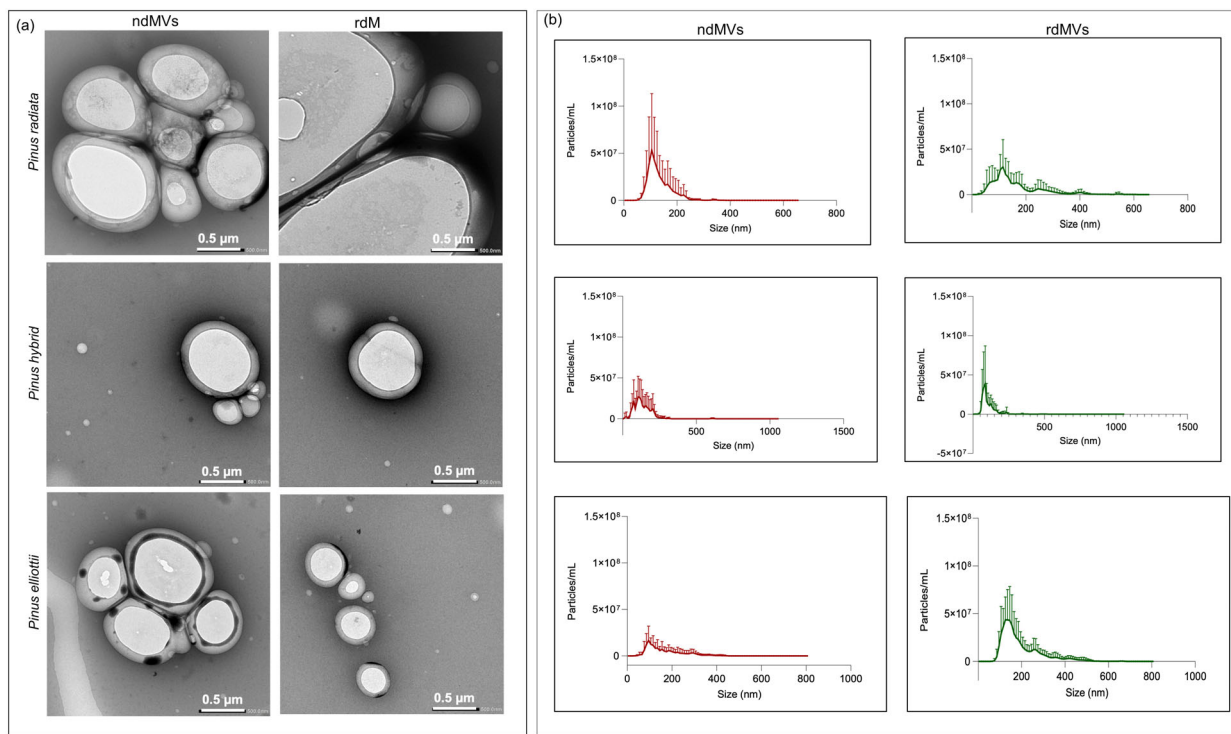


Fig. 1. Characterization of membrane vesicles (MVs) from pine leaves and roots: (a) Transmission electron microscopy (TEM) images revealing the ultrastructure of MVs derived from pine needles (ndMVs) and roots (rdMVs). The images show the intricate details of these vesicles, providing insights into their morphology and composition. (b) Nanoparticle tracking analysis showing size distribution and particle concentration of rdMVs and ndMVs. The graph highlights the range of vesicle sizes and particle concentration. Data from 15 independent biological replicates.

Glasshouse trials following exposure of fungal spores to vesicles

The effect of ndMVs on *P. elliotii* seedlings was also conducted using the FSP34 isolate. These seedlings inoculated with fungal spores served as positive control, while PBS (1×) served as negative control. Two conditions were tested: spores were either washed (ndMVs W) following vesicle exposure or left unwashed (ndMVs UW) for 24 h. This vesicle removal process is key to distinguishing the effects caused directly by the consistent presence of vesicles and effects resulting from the inherent characteristics or virulence factors of the spores internalizing vesicles. SEM was also performed on the needle surface at 14 days post-inoculation with W- and UW-treated spores. Briefly, needles were soaked in methanol overnight so that they were well preserved, then dehydrated, and freed of interfering substances, leading to high-quality SEM images. The needles were then transferred to Eppendorf tubes containing fixative solution (glutaraldehyde) for 30 min to preserve cellular structure. SEM was then performed as previously described. To determine persistence of the infection in pine seedlings post-inoculation, needles and stems were cut after 14 days of inoculation and plated on ¼ PDA plates to assess disease progression. This also included testing non-infected needles and stems to confirm uninfected status.

Data visualization, reproducibility, and statistical analyses

The software R v. 4.4.1. (R Foundation for Statistical Computing) was used to perform correlations, heatmap, and principal

components analysis (PCA) to investigate the effects of PDVs on *F. circinatum* on the PM results (PM1, PM2A, PM3B, PM9, PM24C). Correlation analysis was used to identify relationships between PDVs and *F. circinatum* on the PM variables, while the heatmap visually represented these correlations, highlighting clusters of related effects. PCA was employed to reduce dimensionality and capture primary sources of variance, facilitating identification of trends and potential groupings in the data. Unless otherwise specified, all experimental data were subjected to one-way ANOVA and nonparametric Student's *t*-tests for comparison. Statistical analyses were performed using GraphPad software (GraphPad 5; San Diego, CA, USA). Significance was determined through representation of the mean ± SD with probability thresholds: * $P \leq 0.05$; ** $P \leq 0.002$; *** $P \leq 0.001$; **** $P \leq 0.0001$. Each experiment was conducted with three technical replicates and three biological replicates, unless stated otherwise. Additionally, all experiments included both positive and negative controls to assess the validity and reliability of experimental results.

RESULTS

The physical features of *Pinus* derived vesicles

We used TEM at a magnification of 15,000 (Fig. 1a) to observe physical features of vesicles isolated from seedlings from three different *Pinus* species (*P. radiata* and *P. patula* × *P. tecummanii* = *P. hybrid* and *P. elliotii*). These vesicles were generally free of any inclusions, attached particles, or signs of damage or degradation, which indicates that our protocols for isolating

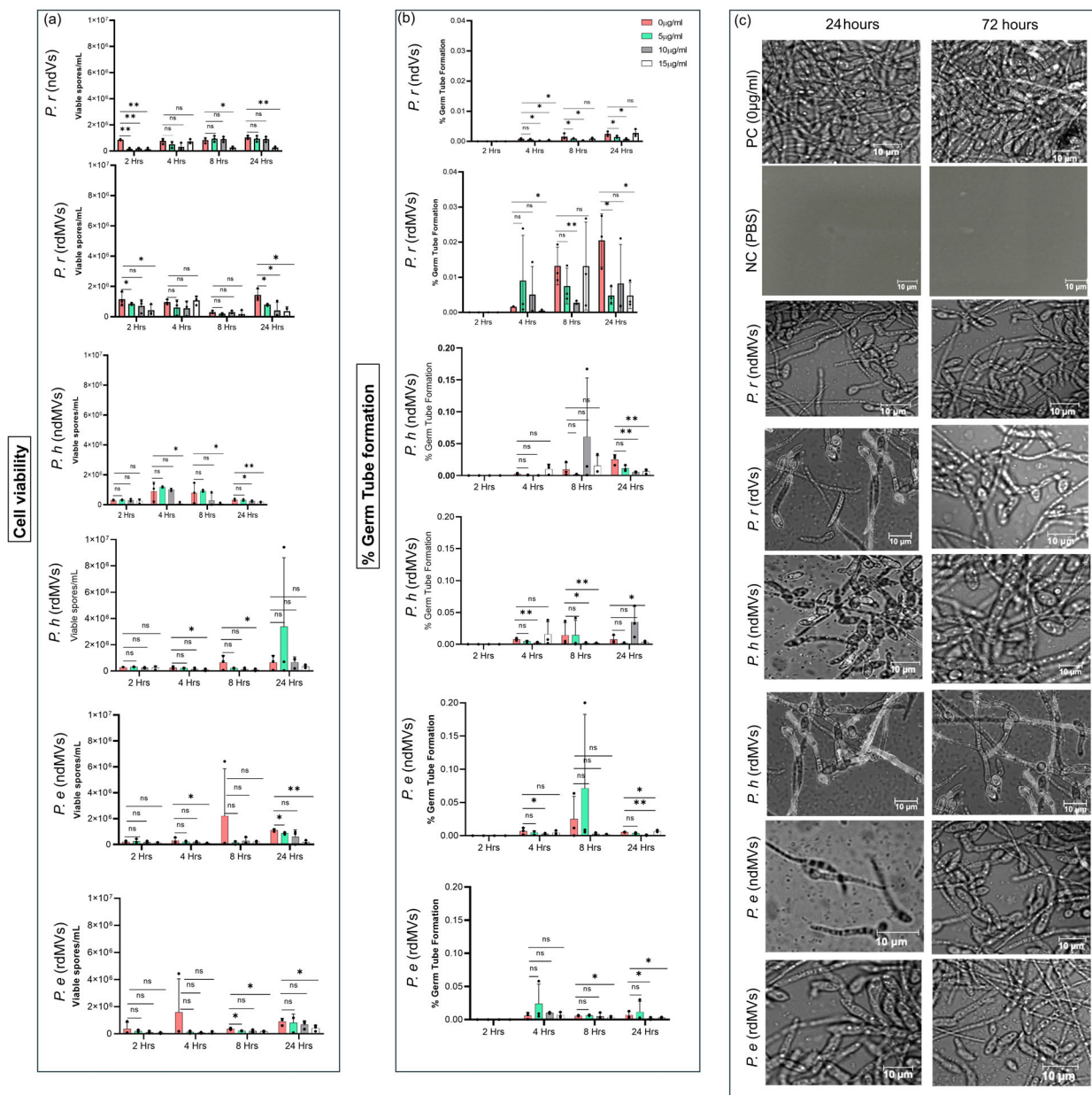


Fig. 2. The influence of membrane vesicles (MVs) on *Fusarium circinatum* hyphal growth in $\frac{1}{4}$ strength potato dextrose broth: comparative effects of needle-derived membrane vesicles (ndMVs) and root-derived MVs (rdMVs) on cell viability (a) and spore germination (b), represented as percentage germ tube formation, and light microscope images (c) showing the effects of vesicles on formation of germ tube after 24 and 72 h at 40 \times magnification. *P. r.*; *Pinus radiata*, *P. h.*; *Pinus hybrid*, *P. e.*; *Pinus elliottii*. Data from 3 independent biological replicates. Scale bar = 10 μ m (c) statistical significance: $P \leq 0.005$; *, $P \leq 0.002$; ***, $P \leq 0.001$; ****, $P \leq 0.0001$; ns, not significant.

vesicles are effective for pine species. Vesicles are generally spherical, with some uniformity in morphology (Fig. 1a). However, slight variations in size were evident among samples. Notably, vesicles from *P. radiata* had a low-density outer layer, whereas *P. elliottii* vesicles had a high-density inner compartment surrounded by a thin dark layer. Despite these differences, vesicles from pine needles and roots showed no major morphological or size distinctions.

NTA was used for measurements of both size and concentration of vesicles, which revealed variations in vesicle size and concentration among samples, with vesicles ranging from 0 nm to 1025 nm (Fig. 1b). However, the majority of vesicles were

within the 0–200 nm size range, indicating a dominant population of small EVs (Fig. 1b). These differences in EV size and concentration highlight variations in vesicle biogenesis pathways, release mechanisms, and potential cellular interactions.

Effects of vesicles on fungal growth of the FSP34 isolate

The FSP34 isolate (CMWF350) of *F. circinatum* was used as primary strain since it is the most pathogenic isolate and is extensively characterized. Use of this strain enables comparisons with existing studies, thus benchmarking against effects of vesicles measured in this study. We first assessed the impact

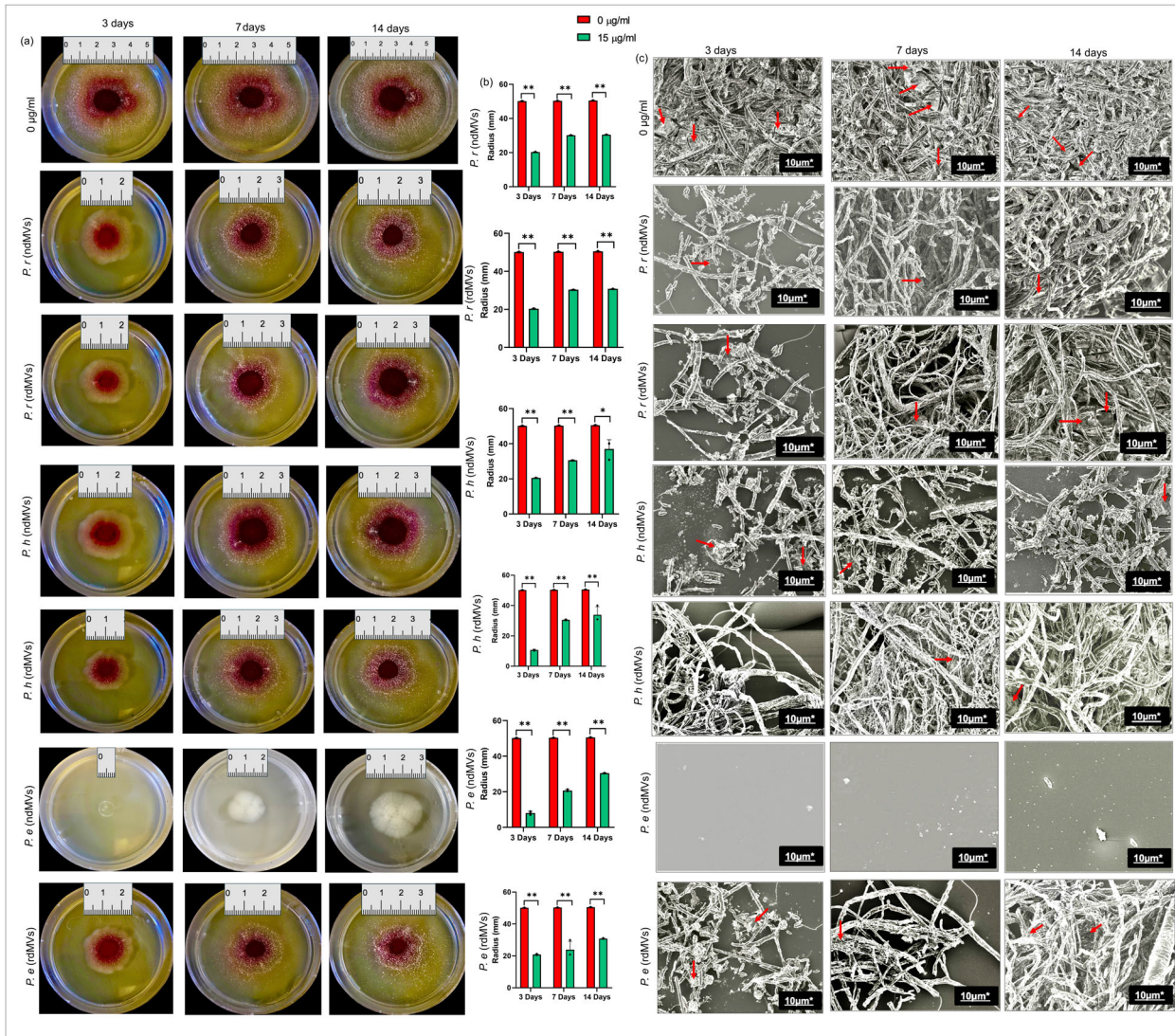


Fig. 3. Phenotypic impact of *Pinus*-derived membrane vesicles (PDMVs) on *F. circinatum* (FSP34) growth on potato dextrose agar. (a) Influence of needle-derived MVs (ndMV) and root-derived vesicles (rdMV) on radial expansion of fungal spores exposed to 15 $\mu\text{g mL}^{-1}$ MVs for 24 h. (b) Quantification of radial growth after treatment with ndMV and rdMV, from 3 independent biological replicates measured as colony diameter (mm). (c) Scanning electron microscope examination of cells collected from the colony periphery on 3-, 7- and 14-day radial growth plates. Cells were examined at 10 \times magnification.

of vesicles on cell viability and germ tube formation in this isolate, which are indicators for fungal host invasion and subsequent pathogenesis. There was significantly lower cell viability and germ tube formation in the 15 $\mu\text{g mL}^{-1}$ vesicle treatment group than in the 5 $\mu\text{g mL}^{-1}$ and 10 $\mu\text{g mL}^{-1}$ vesicle treatment groups (Fig. 2a–c), with the largest reduction in the rdEV treatment group compared to the ndMV treatment group. Specifically, cells treated with vesicles displayed a statistically significant reduction in viability relative to cells not treated with vesicles ($P < 0.001$) (Fig. 2a–c). Similarly, larger cell counts and more germinated spores were observed in control groups than in EV-treated groups ($P < 0.005$) (Fig. 2b,c). These results suggest that vesicles derived from the pine host negatively impact early growth by reducing viable cell counts and the ability of spores to germinate and produce hyphae.

Since PDVs prevented early growth (Fig. 2b,c), we determined whether this effect translates into reduced hyphal

formation (reduction in late growth). We used a plate assay with incubated fungal spores exposed for 24 h to 15 $\mu\text{g mL}^{-1}$ vesicles. The data clearly demonstrated that PDVs inhibit radial growth, as indicated by differences between the control and treatments (Fig. 3a,b). Furthermore, both ndMV and rdV significantly reduced colony growth ($P < 0.001$) (Fig. 3b). PDVs also delayed fungal growth, as colony diameters of vesicle-treated plants were smaller than those of control plants at 7 and 14 days (Fig. 3b).

Both spore germination and hyphal growth reflect ability of the fungus to form biofilms, which are structured, multicellular communities composed of dense hyphal structures enclosed in a matrix (ECM). Therefore, we investigated the ability of *Pinus* vesicles to influence the biofilms of *F. circinatum* since biofilm formation is crucial for survival of this fungus in a range of conditions (Ratsoma *et al.* 2024). Fungal spores previously exposed to vesicles were left to grow as a biofilm at room

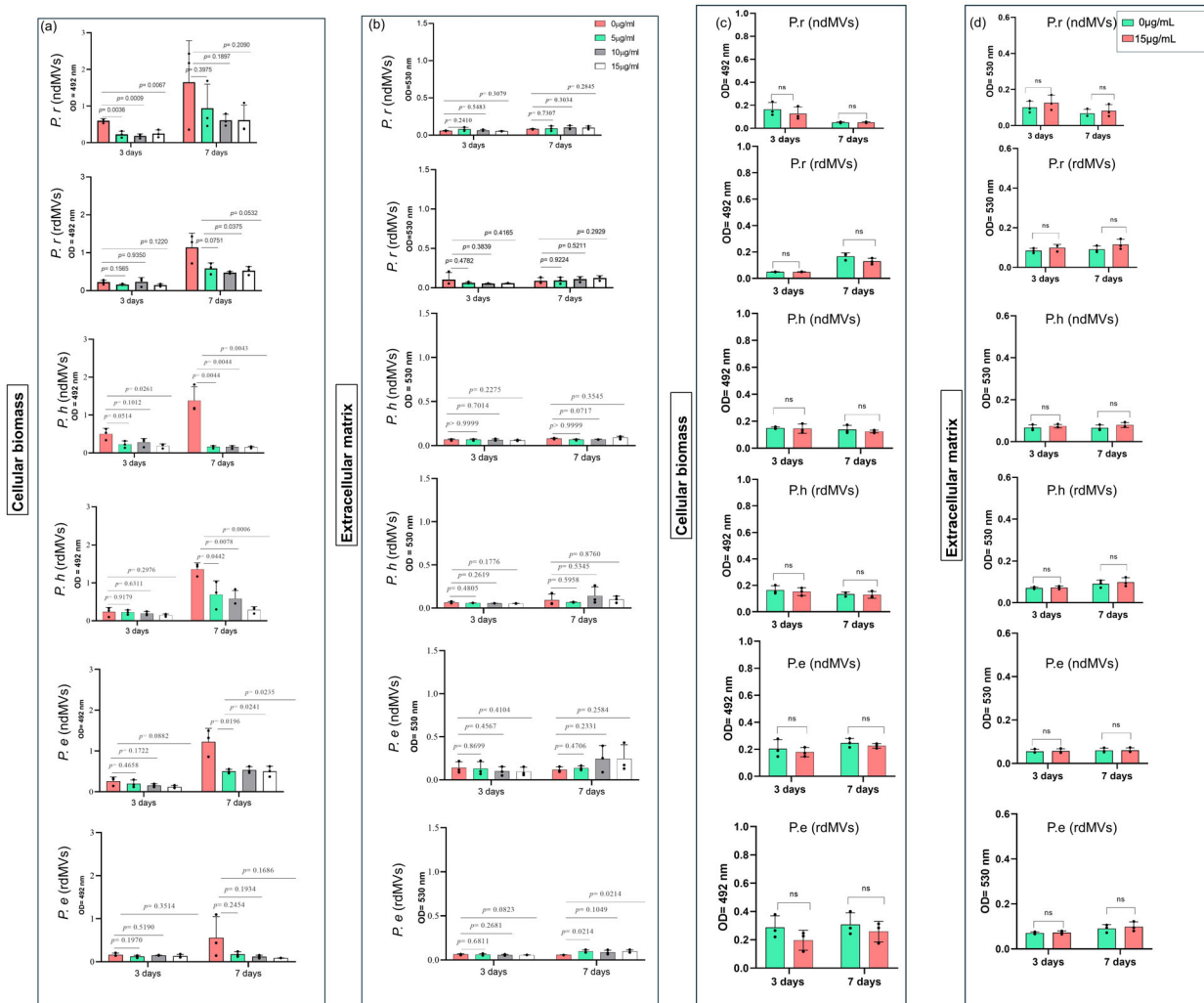


Fig. 4. The influence of needle-derived and root-derived membrane vesicles (ndMVs and rdMVs, respectively) on biofilm biomass (OD = 492 nm) and extracellular matrix (ECM) production (OD = 530 nm). (a) and (b) show effects of rdMVs and ndMVs on biofilm formation, while (c) and (d) show effects on preformed biofilms. Scale bar = 20 μm . P.r = *Pinus radiata*, P.h = *Pinus hybrid*, P.e = *Pinus elliottii*. Data from 3 independent biological replicates. Significance: $P \leq 0.005$: *, $P \leq 0.002$: **, $P \leq 0.001$: ***, $P \leq 0.0001$: ****, $P \leq 0.0001$: ns (not significant).

temperature in PDB (liquid medium). There was a significant decrease in biofilm biomass ($P < 0.001$) (Fig. 4a), suggesting PDVs had a negative effect on fungal cell growth at stationary phase. Despite ability to prevent biofilm biomass production, the vesicles were unable to prevent ECM production (Fig. 4b), suggesting *Pinus* vesicles were unable to eradicate a preformed biofilm of the fungus. To confirm this, we grew the biofilm for up to 7 days and exposed it to $15 \mu\text{g mL}^{-1}$, followed by ECM and biomass determination. The data indicated that neither biofilm component was significantly affected by addition of vesicles (Fig. 4c,d).

Impact of ndMVs on *F. Circinatum* global nutrient profile

The ndMVs broadly impact FSP34 metabolism

To further reveal the effects of ndMVs on the primary strain (*F. circinatum* FSP34), we used phenotypic microarray analysis (Figs. 6–8). These microarrays revealed preferences of the fungus (vesicle-condition) for various carbon sources (PM1,

PM2A) (Fig. 5a–d), nitrogen sources (PM3B) (Fig. 5e,f), osmolytes (PM9) (Fig. 6a,b), and chemicals (PM24C) (Fig. 6c,d). However, this was influenced by treatment of fungal spores with ndMVs of *P. elliottii*, with significant metabolic shifts in all PM plates under EV+ conditions (Figs. 5 and 6). For instance, in PM1 (Fig. 5), there was significant metabolic suppression, particularly affecting key carbon sources, e.g., D-glucose, maltose, and D-galactose, showing a shift from high activity (dense blue) in the (-Vs) condition to low activity (gradient red) in the (+Vs) condition. This finding suggests that ndMVs interfere with central carbohydrate metabolism, potentially disrupting glycolysis and related pathways crucial for energy production and growth. Nitrogen and phosphorus metabolism were also heavily impacted in the +MVs condition of PM2A (Fig. 5), with compounds such as D-serine, glycyl-L-glutamic acid, and D-alanine, indicating interference with nitrogen assimilation. Similar suppression was observed in amino acid metabolism in the +MVs condition of PM3B (Fig. 5), affecting L-aspartic acid and L-cysteine, while other

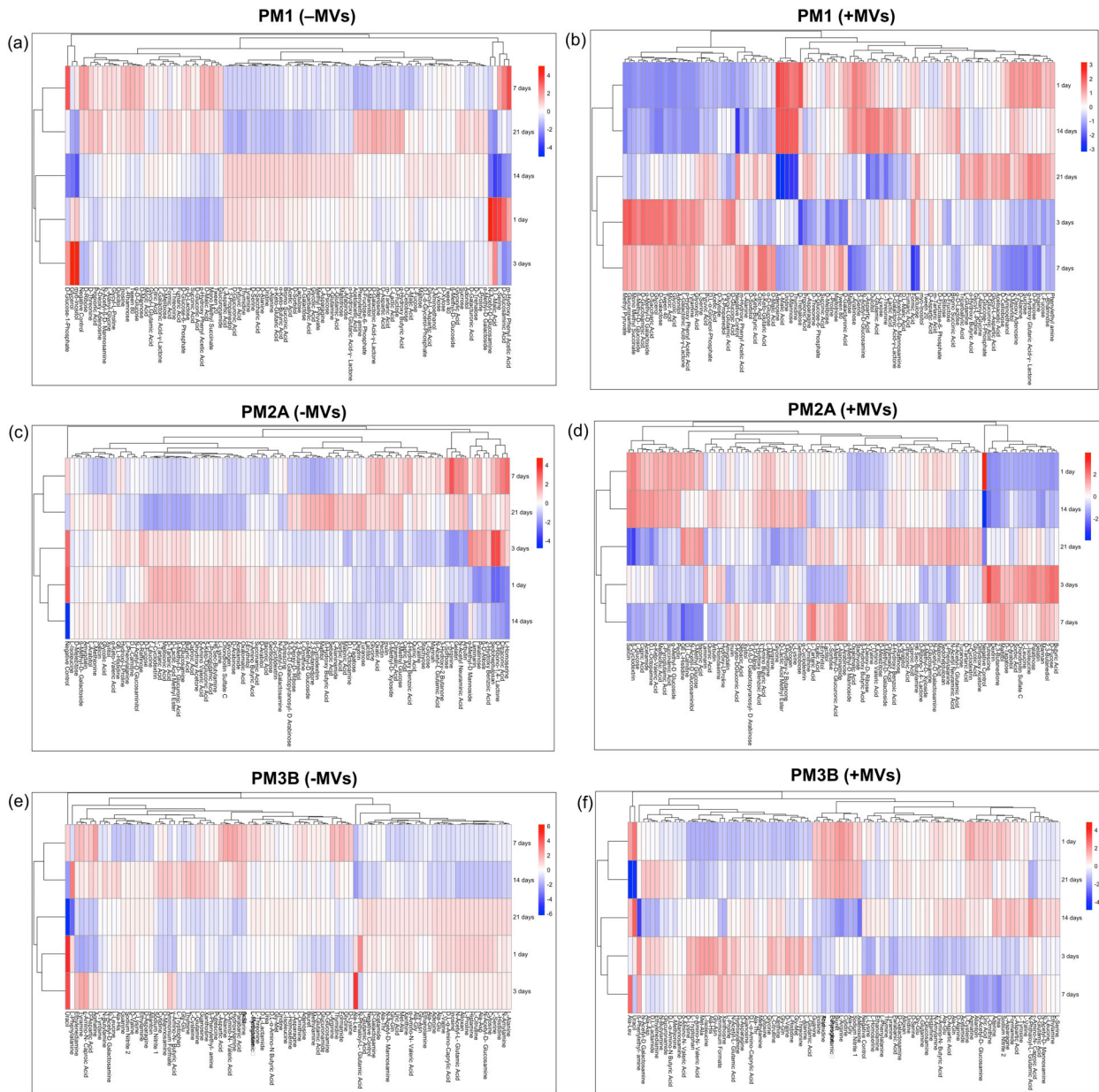


Fig. 5. Metabolic activity of *Fusarium circinatum* free spores (-MVs) and MVs-exposed spores (+MVs) following growth on carbon sources (PM1, PM2A (a–d)) and nitrogen sources (PM3B (e,f)). Data from 3 independent biological replicates from time points 1, 3, 7, 14, and 21 days. Each row corresponds to a specific carbon or nitrogen source, with colour intensity reflecting the extent of nutrient utilization.

compounds (e.g., L-Citrulline) had increased activity, suggesting metabolic adaptation. In PM9 MV+ (Fig. 6), there was early strong suppression of osmolyte metabolism, including glycine betaine and trehalose, with partial recovery by day 7. In PM24C MV+ (Fig. 6), the heatmaps showed initial broad suppression of chemical stress tolerance, with sodium metasilicate and sodium fluoride significantly inhibition, followed by recovery at later stages for some antimicrobials.

The ndMVs induce temporal and disorganized metabolic responses

The PCA of responses during growth in phenotypic microarray plates revealed significant time-dependent metabolic changes

between +MV and -MV fungal spore groups (Fig. 7). At early time points (day 1 and day 3), there was minimal separation between the two groups, with substantial overlap between clusters, suggesting that both groups underwent similar initial metabolic adjustments. This early phase likely represents an adaptation period before vesicles exert full effects on fungal metabolism. By day 7, clear separation between +MV and -MV clusters began to emerge, reflecting metabolic shifts and the onset of stress responses in +MV spores. These differences became more pronounced by days 14 and 21, with +MV clusters exhibiting greater dispersion compared to the more tightly grouped -MV clusters. This group maintained more consistent metabolic profiles across all time points, as reflected in the

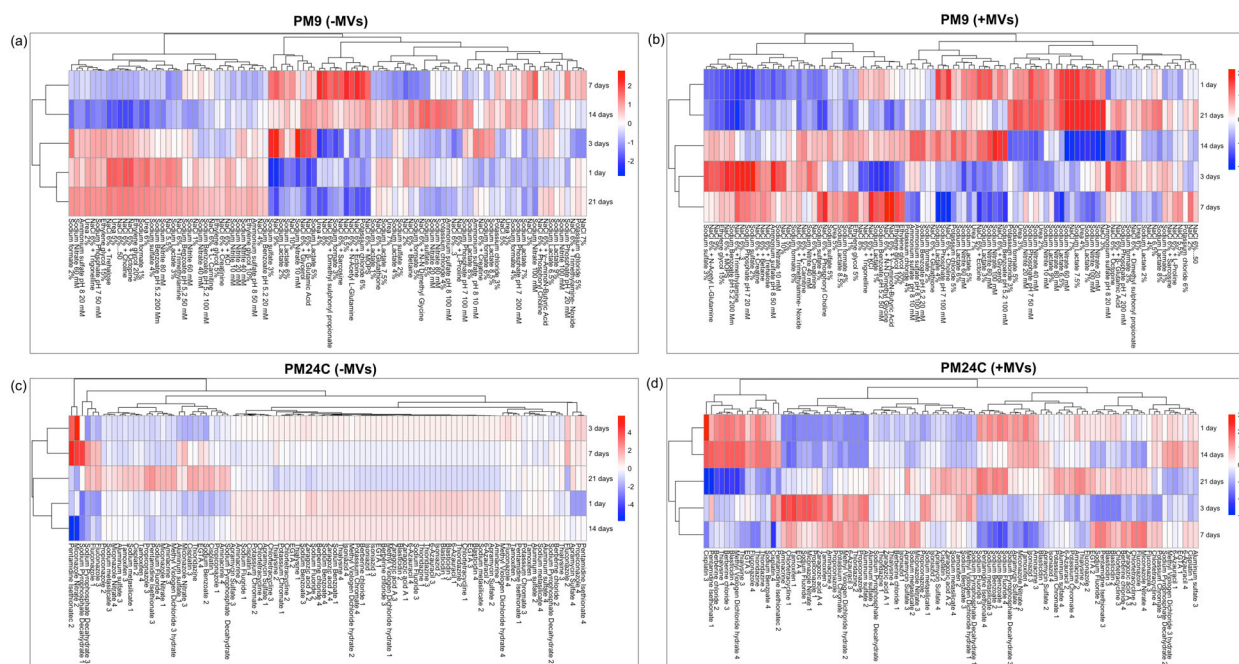


Fig. 6. Metabolic activity of *Fusarium circinatum* spores free of needle-derived membrane vesicles (-MVs) and spores exposed to membrane vesicles (+MVs) following growth on osmolytes (PM9 (a,b), and chemicals (PM24C (c,d)). Data from 3 independent biological replicates and time points of 1, 3, 7, 14, and 21 days. Each row corresponds to a specific carbon or nitrogen source, with colour intensity reflecting the extent of nutrient utilization.

tighter clustering pattern. This consistency suggests stable metabolic activity and a lack of significant stress accumulation in the absence of vesicle treatment.

Overall, the metabolic profile in the (+MVs) group PCA plots shows highly disorganized metabolism (e.g., energy production, reduced stress tolerance, and inefficient carbon utilization related to ndMVs). To identify metabolic pathways with these shifts, we used correlation heat maps (Fig. S2) using PM1, PM3B, and PM24C as examples. The data strongly suggest significant correlation shifts in the +MV condition pertaining to disrupted interactions in compounds of glycolysis and the TCA cycle (e.g., pyruvic acid and citric acid; energy metabolism), amino acid biosynthesis (e.g., L-glutamate, L-proline, and L-serine), lipid and membrane component metabolism (e.g., *N*-acetyl-D-glucosamine, a building block of chitin), and antioxidant and stress-related metabolism (e.g., myo-Inositol and tween). The reduced overall mean correlation among many metabolites was also observed in the +MV condition, likely further reflecting the loss of cohesive functionality in the fungus and, hence, inability to effectively utilize compounds present in the PM plates (Fig. S2). Therefore, the presence of ndMVs also resulted in severe disruptions to metabolic synchronization.

The ndMVs improve *Pinus* seedling health

Since there were inhibitory effects of $15 \mu\text{g mL}^{-1}$ ndMVs on filamentous growth, we assessed whether exposure to these vesicles can reduce the ability of spores to cause infections. We conducted glasshouse trials in which *P. elliotii* plants were infected with *F. circinatum* FSP34 spores previously exposed to $15 \mu\text{g mL}^{-1}$ ndMVs for 24 h. Some of these spores were

subjected to vesicle removal by washing with PBS. Seedlings exposed to ndMVs without washing (UW) or with washing (W) after 24 h showed varying degrees of disease resistance (Fig. 8). Notably, when seedlings were inoculated with UW spores, they had better health and growth than the washed seedlings (W) and the positive control, especially between 3 and 7 days post-inoculation (dpi). This indicates that the continuous presence of ndMVs on seedlings enhanced seedling resistance to infection (Fig. 8a).

Seedlings inoculated with UW and W spores had distinct differences in disease resistance and overall health at 3, 7, and 14 dpi (Fig. 8b). The observed reduction in lesion length and disease severity index, coupled with increased chlorophyll content, highlight the effectiveness of ndMVs in preventing seedling infections and maintaining seedling health (Fig. 8b). In contrast, the washed group (W), in which ndMVs were removed from fungal spores after the initial 24-h exposure, showed reduced resistance at 14 dpi, indicating that transient presence of ndMVs is not sufficient to confer long-term resistance. In addition, the chlorophyll content was consistently higher in both UW and W needles than in the positive control needles throughout the 14-day observation period. Notably, chlorophyll levels were highest at 3 dpi and gradually decreased by day 14 in both treatments. Despite this decline over time, the chlorophyll content in the UW and W needles remained significantly higher than that in control needles across all time points, indicating that exposure to ndMVs positively impacts chlorophyll retention and overall plant health.

An SEM was then used to visualize surface morphology of needle tissues after different treatments (Fig. 8c). This revealed that control seedlings (control ($0 \mu\text{g mL}^{-1}$), top panel),

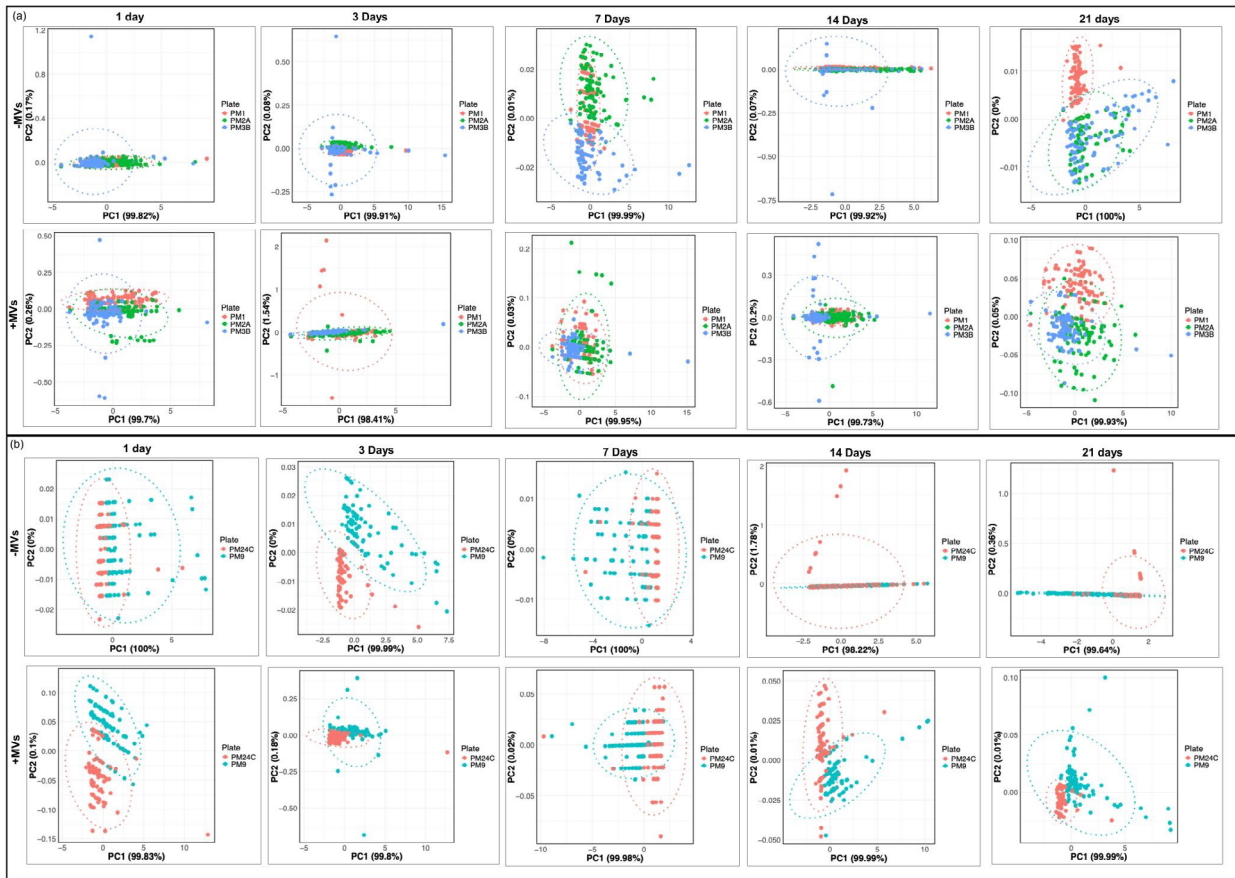


Fig. 7. PCA of carbon and nitrogen sources (PM1, PM2A, and PM3B) (a) and osmolytes (PM9) and chemicals (PM24C) (b) illustrating *Fusarium circinatum* metabolic responses under membrane vesicle treatment (+MV) and without the treatment (-MV) at day 1, 3, 7, 14, and 21. At early time points (days 1 and 3), clusters overlap, suggesting similar metabolic adjustments in both (+MV) and (-MV) groups. From day 7 onward, distinct separation, with +MV groups showing increased variability, indicating metabolic disruption, particularly in carbohydrate, amino acid, and nitrogen metabolism. Data from 3 independent biological replicates.

subjected to ndMVs-free spores, had atypical surface architecture, with signs of extensive damage with distorted and irregular surface features. In contrast, the SEM image of seedling tissue inoculated with UW spores treated with ndMVs (*P. elliotii* (ndMVs), bottom panel) had a smoother and uniform surface, suggesting that ndMVs might protect tissues from effects of pathogenic spores. Furthermore, stomata were clearly visible and less clogged or distorted, indicating that the invasion of spores was halted by ndMVs. In control plants, stomata were irregular and possibly disrupted.

To determine persistence of the infection in pine seedlings post-inoculation, needles and stems were cut 14 days after inoculation and plated on ¼ PDA plates (Fig. S3). This test included uninfected needles and stems to confirm uninfected status. Needles and stems from infected plants continued to show fungal growth, with reduced pigmentation, typical of *F. circinatum*, indicating persistent infection (Fig. S3a). Furthermore, analysis of plate growth showed that growth of *F. circinatum* in non-inoculated needles and stems was more rapid than in the ndMVs groups and the negative control, indicating that infection is more severe in infected seedlings. Pre-treatment of fungal spores with ndMVs might have influenced microbial communities colonizing the various pine

seedling tissues (needles and stems), as with different non-*circinatum* fungi (i.e., fungi different from 'control') between all the seedling (i.e., those infected with spores pre-treated with PBS and ndMVs (W and UW)) and tissue groups (stem and needle). Indeed, the appearance of non-*circinatum* isolates, which may be endophytic or opportunistic, suggests selective fungistatic effects of ndMVs, which possibly allowed growth of beneficial fungi. Therefore, our data suggest that the competitive landscape is significantly affected when *F. circinatum* growth is altered by ndMVs, potentially allowing beneficial microbes to emerge. Thus, the impact of ndMVs on microbial communities should be thoroughly investigated.

The ndMVs inhibit filamentous growth in field isolates

We further investigated whether ndMVs from *P. elliotii* have the same or different effects on other field isolates of *F. circinatum* by studying radial growth of three strains (CMWF2654, CMWF2552, CMWF5689) following spore treatment with 15 µg mL⁻¹ vesicles (Fig. S4a-c). Since these isolates are from different provinces of South Africa (Table S1), they represent broader genetic diversity and varying responses to vesicle

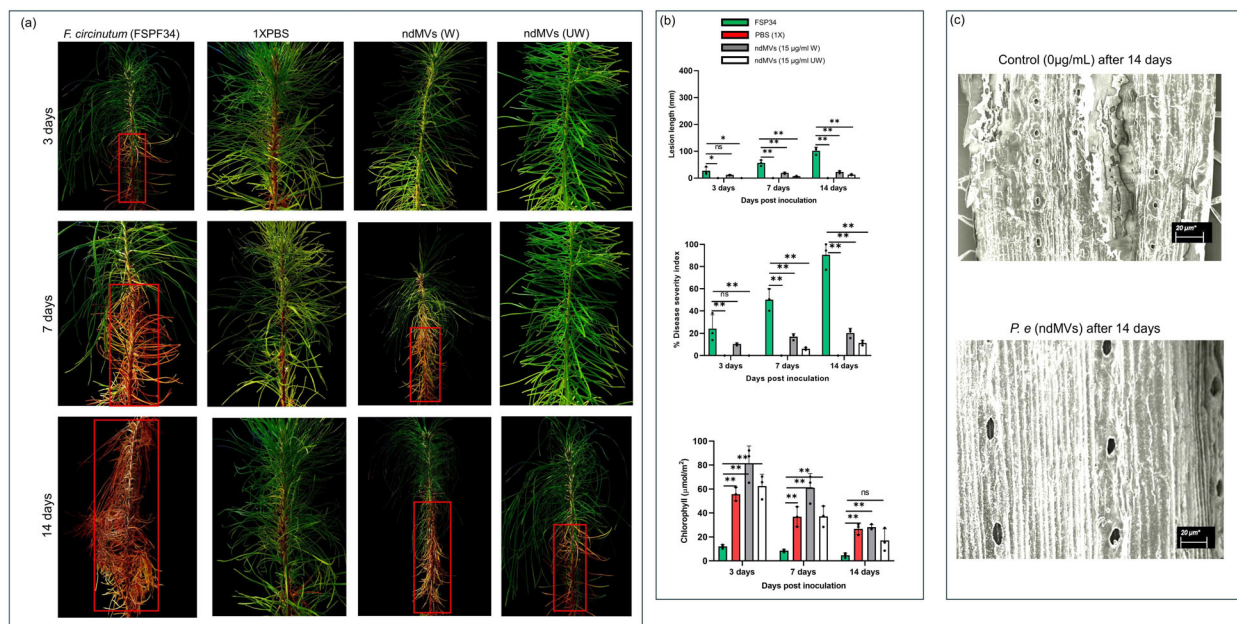


Fig. 8. Inoculation trial on pine seedlings with *F. circinatum* (FSPF34) as positive control and PBS (1×) as negative control. Seedlings were treated with $15 \mu\text{g mL}^{-1}$ *Pinus elliotii* needle-derived membrane vesicles (ndMVs). Three independent biological replicates included spores treated with ndMVs not subjected to vesicle removal process (unwashed or UW) and those washed of residual vesicles following ndMVs treatment (W) after 24 h (a). Seedling growth and health were monitored over 3, 7, and 14 days by measuring lesion length, % disease severity index, and chlorophyll content (b). Scanning electron microscope (SEM) examination of the influence of MVs on needles after 14 days post-inoculation at 2× magnification (c).

exposure because of their different evolutionary background and environmental adaptations. The radial growth in colonies of these isolates was quantified over 14 days (Fig. S4a,b), during which the control groups ($0 \mu\text{g mL}^{-1}$) served as baseline for radial growth comparison. We observed a trend similar to that after *F. circinatum* FSP34, with significant reductions in radial growth and, in some cases, loss of pigmentation, and colonies similar to those growing out of yeast cells. Interestingly, CMWF2552 showed little growth after 14 days, suggesting it is highly sensitive to treatment with vesicles. Significant differences in growth were also observed between the control and treatment groups (Fig. S4b). Light microscopy showed that hyphal growth minimal in the treatment groups (Fig. S4c). These data suggest that the ndMVs of *P. elliotii* inhibit not only growth and pigmentation of *F. circinatum* FSP34 (Fig. 3), but also growth of field isolates of this pathogen. Since there was variability in the response of different strains of *F. circinatum*, our data suggest a possible wide range of genetic and physiological outcomes in fungi.

The ndMVs inhibit growth in non-*circinatum* fungal species

Given results from *F. circinatum*, we further investigated whether these vesicles inhibit pathogens from other filamentous fungal species. We assessed radial colony growth of selected fungal isolates (Table S1), including *B. cinerea*, *Chrysosporthe cubensis*, and two *Fusarium* species (CMWF2652, and CMW59120), over 14 days. There was a significant reduction in colony growth with increasing concentrations of ndMVs treatment, with more pronounced effects over time (Fig. S5). For *B. cinerea* (Isolate CMW13135), the colony radius decreased significantly compared to the control at both treatment concentrations from day 3 to day 14 (Fig. S5a,b). Similar

trends were observed in *F. graminearum* (CMW58100) and *F. verticillioides* (CMW59120), where higher concentrations of ndMVs led to marked reductions in colony growth (Fig. S5e–h).

DISCUSSION

We isolated and characterized vesicles from *Pinus* spp., an important step in understanding how vesicle-mediated communication influences pine–microbe interactions. Using SEC, we purified vesicles from crude extracts of pine needles and roots, yielding both small and large vesicles. However, the most abundant vesicle size in both root and needle preparations was around 200 nm, suggesting that the vesicle effects reported here are predominantly induced by small vesicles. Studies on other plants, such as *Arabidopsis* and rice, have reported similar MV size ranges, indicating that size regulation may be a common feature across species (Kalluri & LeBleu 2020; Liu *et al.* 2020; Wu *et al.* 2024). According to particle analysis, MVs from needles (ndMVs) and roots (rdMVs) were generally similar in size. Additionally, TEM analysis revealed structural features, including a distinct surrounding layer, consistent with characteristics reported in other studies (De Palma *et al.* 2020). Collectively, these findings provide a foundation for investigating the functional significance of vesicle size and morphology in intercellular and long-distance communication during plant–microbe interaction.

Needle- and root-derived MVs were bioactive, both inhibiting the viability of spores in *F. circinatum*, suggesting compounds within these vesicles may interfere with early-growth processes, such as spore germination (Regente *et al.* 2017; Schlemmer *et al.* 2022). The inhibitory action of vesicles was also observed in other filamentous pathogens, including those

reported to be inhibited by ndMV and rdMV of *P. patula* and rdMVs of tomato (De Palma *et al.* 2020; Motaung *et al.* 2025). Therefore, it would be interesting to test vesicle preparations from non-host plants on *F. circinatum* to explore whether they exhibit similar antifungal effects, further expanding the potential of plant-derived vesicles as biocontrol agents.

We further investigated the impacts of fungal exposure to vesicle preparations using phenotypic microarrays (PMs), which revealed severe MV-induced metabolic deficits in *F. circinatum*. Although the role of MVs in modulating cellular phenotypes has been found (Ene *et al.* 2016; Kalvala *et al.* 2019), PM studies focusing on filamentous plant pathogens are limited even though they complement data generated through next generation sequencing. Therefore, our study provide the first comprehensive phenotypic microarray profile induced by MVs. Tanzer *et al.* (2003) and Ene *et al.* (2016) investigated fungal response to nutrient availability, while our PM work demonstrates that ndMVs target key pathways in the fungus, impairing use of carbon and nitrogen sources, and predisposing the fungus to a range of stressful conditions. Therefore, our PM data represent a significant advance in both fungal biology and understanding the multifaceted interactive effects of vesicles.

Furthermore, vesicles had notable inhibitory effects on fungal pigmentation in both the primary strain (FSP34) and in field isolates. Pigmentation plays an important role in the adaptive response of fungi. For instance, melanin production can protect fungal cells from chemical toxicity and UV radiation (Cordero & Casadevall 2017). In our PM study, growth on amino acids (e.g., tyrosine and phenylalanine), vitamins and cofactors (e.g., biotin and niacin), and trace elements (copper and iron) in various PM plates was greatly inhibited. These compounds are important in biosynthetic pathways that contribute to pigment production in fungi. In addition, various carbohydrates in PM1 and PM2A, which the fungus failed to utilize following vesicle treatment, might be required for energy during biosynthesis of pigments (Bleackley *et al.* 2020; Schlemmer *et al.* 2022).

Fungi treated with fungicides and plant-derived natural compounds (e.g., essential oils), targeting ergosterol biosynthesis, mitochondrial respiration, and osmoregulation (Wu & von Tiedemann 2002; Becher & Wirsal 2012), display metabolic effects similar to those observed in this study. However, conventional fungicides and novel small molecules (e.g. imidazopyrazoindoles) target specific metabolic or membrane pathways. On the other hand, *Pinus*-derived vesicles disrupt multiple metabolic processes simultaneously, rendering MVs similarly effective as combination therapy. These may also sensitize the fungus to the inhibitory effects of multiple fungicides, including azoles (present in the PM24C plate). This implies that application of *Pinus* vesicles can reduce reliance on high doses of chemicals during agricultural disease control. Our glasshouse findings demonstrated that MVs *in vitro* have a significant positive impact on disease response in pine seedlings. Studies using leaf detachment assays have reported similar protective effects (Liu *et al.* 2021; McMillan *et al.* 2021; Zhang *et al.* 2022). Therefore, our findings expand upon previous studies by confirming, in a controlled glasshouse setting, that these vesicles have potential for improving plant health, contributing to disease resistance in whole plants. In future, these results will have applications in agricultural practices to promote plant health and forestry management of pathogens.

In conclusion, *Pinus* vesicles likely deliver a blend of inhibitory molecules (e.g., RNAs, enzymes, antimicrobial peptides) that collectively compromise fungal physiology. This offers a promising strategy for preventing infections and enhancing plant defence mechanisms, as demonstrated in the glasshouse trials. Moreover, the same set of seedlings from which inhibitory ndMVs were extracted were unable to protect themselves from *F. circinatum*, despite their isolated vesicles having antifungal effects. Several factors might explain this discrepancy, including the natural concentration of vesicles within pine tissues, which could be insufficient to achieve lab-level inhibition, the internal environment of an infected seedling, which could impair the bioactivity of vesicles, as well as the timing of vesicle release and the specific *in planta* locales in which vesicle activity is optimal. Future studies should focus on quantifying the *in planta* and infection site concentrations of vesicles and highlight potential *in planta* modifications that might promote the stability and efficacy of vesicles. While ecologically valuable in its native range, *P. elliottii* may become a problematic invader in regions like South Africa, where its rapid spread could potentially displace native biodiversity and disrupt ecosystem balance (Richardson & Rejmánek, 2011). Therefore, large-scale harvesting of MVs from this pine species could help curb the tree's invasive spread by utilizing detached biomass productively, aligning with emerging "biocircular" approaches to invasive species control. This intriguing nexus between invasion biology and biochemical properties opens unique opportunities to innovate and restore ecosystems through the application of bioactive MVs.

AUTHOR CONTRIBUTIONS

SK performed the experiments, analysed the data, wrote the original manuscript, and wrote and edited the manuscript. TM designed the study, formal analysis, funding acquisition, investigation, methodology, project administration, resources, supervision, and provided feedback on the manuscript. ES contributed to the data analysis, supervision, and interpretation and provided feedback on the manuscript. All authors contributed to writing and reviewing the manuscript.

ACKNOWLEDGEMENTS

Funding was provided by the South African National Department of Science and Innovation-NRF under the Thuthuka funding instrument (Grant no. 129580) and the Centers of Excellence programme and South African Research Chairs Initiative (Grant no. 98353). We extend our gratitude to the Laboratory for Microscopy and Microanalysis, Department of Veterinary Tropical Diseases, University of Pretoria, Onderstepoort Campus, South Africa, for assistance with transmission electron microscopy, and the Council for Scientific and Industrial Research (CSIR), Pretoria, South Africa, for assistance with Nanoparticle tracking analysis. We further express our heartfelt appreciation to Linience Maphosa for the invaluable training provided for SEC. We are equally grateful to our dedicated student mentees, Sikhumbule Ncanywa (2023) and Zoe Odendaal (2024), for their commitment and hard work. Special thanks also go to Sandra Vanwyngaard for assistance with BCA training.

CONFLICTS OF INTEREST STATEMENT

None.

SUPPORTING INFORMATION

Additional supporting information may be found online in the Supporting Information section at the end of the article.

Data S1. Supporting Information.

Fig. S1. Overview of membrane vesicle (MVs) isolation process from pine needle and root juice. (A, B) Pine leaves and roots cleaned and dried (C). Dried plant material mixed with vesicle isolation buffer (D). Juice extracted, filtered (E), and loaded into centrifuge tubes (F). Centrifugation at $700 \times g$ to remove plant fibres (G), followed by filtration through a $0.22\text{-}\mu\text{m}$ membrane (H). A second centrifugation at $8000 \times g$ concentrates fluid (I), removing excess buffer (J), then placed into Eppendorf tubes (K). (L) concentrated supernatant mixed with lipophilic dye FM4-64 and incubated (M). The sample is loaded onto a Sepharose CL2B column equilibrated with phosphate-buffered saline (PBS) (N). Fractions ($200\ \mu\text{L}$) collected in 96-well plates (O), and fluorescence measured using a spectra max M2 plate reader (P). Fractions >3.3 RFU pooled, indicating presence of vesicles.

Fig. S2. Correlation matrices of metabolite interactions across different PM plates (PM1, PM3B and PM24C), comparing treatments with (+MVs) and without vesicles (-MVs). Each subplot displays correlation coefficients (-1 to 1) among metabolites in different conditions, with positive correlations

in red shades and negative correlations in blue shades. Strong positive or negative correlations in darker shades. Matrices highlight shifts in metabolite interactions potentially induced by vesicle treatment, illustrating how vesicles influence metabolic pathways over 1, 3, 7, 14, and 21 days. Data from 3 independent biological replicates.

Fig. S3. Disease persistence on needle and stem samples after 14 days post-inoculation. Needles (a) and stems (b) plated on $\frac{1}{4}$ potato dextrose agar (PDA) plates after 14 days to check for disease growth and effect on microbial communities. Data from 3 independent biological replicates.

Fig. S4. Radial growth of fungal colonies of other *Fusarium* strains (CMWF2552, CMWF2654, CMWF5689) over 14 days on PDA plates following a 24 h exposure to $15\ \mu\text{g mL}^{-1}$ needle-derived membrane vesicles (ndMVs). Fungal spores were incubated with ndMVs and controls without ndMVs. Growth measured in 3 independent biological replicates at 3, 7, and 14 days to determine the impact of ndMVs on fungal proliferation (a,b). Light microscopy of vesicle-exposed and non-exposed cells (controls) on PDA plates at 3, 7 and 14 days (c). Plates examined at 20x magnification. P.r; *Pinus radiata*, P.h; *Pinus* hybrid, P.e; *Pinus elliotii*. scale bar = $20\ \mu\text{m}$.

Fig. S5. Radial growth of fungal colonies of *Botrytis cinerea* (a,b), *Chrysosporthe cubensis* (c,d), *Fusarium graminearum* (e,f), *Fusarium circinatum* CMWF 2652 (g,h), *Fusarium verticillioides* (I,j) over 14 days on $\frac{1}{4}$ potato dextrose agar plates following a 24 h exposure to $15\ \mu\text{g mL}^{-1}$ and $30\ \mu\text{g mL}^{-1}$ *P. elliotii* needle-derived membrane vesicles, respectively. Schematic representation of radial growth (mm) with $\pm\text{SD}$ (b, d, f, h, j). Data from 3 independent biological replicates.

REFERENCES

- Badik K.J., Jahner J.P., Wilson J.S. (2018) A biogeographic perspective on the evolution of fire syndromes in pine trees (*Pinus*: Pinaceae). *Royal Society Open Science*, **5**, 172412. <https://doi.org/10.1098/rsos.172412>
- Barreto-Vieira D.F., Barth O.M. (2015) Negative and positive staining in transmission electron microscopy for virus diagnosis. *Microbiology in Agriculture and Human Health*, **16**, 45–56. <https://doi.org/10.5772/60511>
- Becher R., Wirsal S.G. (2012) Fungal cytochrome P450 sterol 14α -demethylase (CYP51) and azole resistance in plant and human pathogens. *Applied Microbiology and Biotechnology*, **95**, 825–840. <https://doi.org/10.1007/s00253-012-4195-9>
- Bleackley M.R., Samuel M., Garcia-Ceron D., McKenna J.A., Lowe R.G., Pathan M., Zhao K., Ang C.S., Mathivanan S., Anderson M.A. (2020) Extracellular vesicles from the cotton pathogen *Fusarium oxysporum* f. sp. *vasinfectum* induce a phytotoxic response in plants. *Frontiers in Plant Science*, **10**, 1610. <https://doi.org/10.3389/fpls.2019.01610>
- Böing A.N., Van Der Pol E., Grootemaat A.E., Coumans F.A., Sturk A., Nieuwland R. (2014) Single-step isolation of extracellular vesicles by size-exclusion chromatography. *Journal of Extracellular Vesicles*, **3**, 23430. <https://doi.org/10.3402/jev.v3.23430>
- Cai Q., Qiao L., Wang M., He B., Lin F.M., Palmquist J., Scholthof H.B., Jin H. (2018) Plants send small RNAs in extracellular vesicles to fungal pathogens to silence virulence genes. *Science*, **360**, 1126–1129. <https://doi.org/10.1126/science.aar44142>
- Cordero R.J.B., Casadevall A. (2017) Functions of fungal melanin beyond virulence. *Fungal Biology Reviews*, **31**, 99–112. <https://doi.org/10.1016/j.fbr.2016.12.003>
- De Palma M., Ambrosone A., Leone A., Del Gaudio S., Ruocco M., Piccirillo P., Turiak L., Bokka R., Pocsfalvi G. (2020) Plant roots release small extracellular vesicles with antifungal activity. *Plants*, **9**. <https://doi.org/10.3390/plants9121777>
- Ene I.V., Lohse M.B., Vladu A.V., Morschhäuser J., Johnson A.D., Bennett R.J. (2016) Phenotypic profiling reveals that *Candida albicans* opaque cells represent a metabolically specialized cell state compared to default white cells. *MBio*, **7**, e01269-16. <https://doi.org/10.1128/mBio.01269-16>
- Gámez-Valero A., Monguió-Tortajada M., Carreras-Planella L., Franquesa M., Beyer K., Borràs F.E. (2016) Size-exclusion chromatography-based isolation minimally alters extracellular vesicles' characteristics compared to precipitating agents. *Science Reports*, **6**, 33641. <https://doi.org/10.1038/srep33641>
- Gardiner C., Di Vizio D., Sahoo S., Théry C., Witwer K.W., Wauben M. (2016) Techniques used for the isolation and characterization of extracellular vesicles: Results of a worldwide survey. *Journal of Extracellular Vesicles*, **5**, 32945. <https://doi.org/10.3402/jev.v5.32945>
- Hansen E.M., Lewis K.J., Chastagner G.A. (Eds) (2018) Appendix: Diseases of conifers, *Compendium of conifer diseases*, 2nd edition. APS Press, St. Paul, MN, pp 183–220.
- Kalluri R., LeBleu V.S. (2020) The biology, function, and biomedical applications of exosomes. *Science*, **367**. <https://doi.org/10.1126/science.aau6977>
- Kalvala A., Wallet P., Yang L., Wang C., Neelapu S.S., Watowich S.S., Westin J.R., Wargo J.A., Sharma P. (2019) Phenotypic switching of naïve T cells to immune-suppressive Treg-like cells by mutant KRAS. *Journal of Clinical Medicine*, **8**. <https://doi.org/10.3390/jcm8101726>
- Liu G., Kang G., Wang S., Cheng L., Zhang X., Zhao Y., Xu J., Zhang X., Sun X., Zhang W. (2021) Extracellular vesicles: Emerging players in plant defense against pathogens. *Frontiers in Plant Science*, **12**, 757925. <https://doi.org/10.3389/fpls.2021.757925>
- Liu N.J., Wang N., Bao J.J., Zhao J., Zhu H., Yu L., Lu X., Wang Y., Hou Y. (2020) Lipidomic analysis reveals the importance of GIPCs in *Arabidopsis* leaf extracellular vesicles. *Molecular Plant*, **13**, 1523–1532. <https://doi.org/10.1016/j.molp.2020.07.016>
- McMillan H.M., Zebell S.G., Ristaino J.B., Dong X., Kvitko B.H., He S.Y. (2021) Protective plant immune responses are elicited by bacterial outer membrane vesicles. *Cell Reports*, **34**, 108645. <https://doi.org/10.1016/j.celrep.2020.108645>
- Morris A.R. (2022) Changing use of species and hybrids in south African forest plantations. *Southern Forests: a Journal of Forest Science*, **84**, 193–205. <https://doi.org/10.2989/20702620.2022.2110538>
- Motaung T.E., Ratsoma F.M., Kunene S., Santana Q.C., Steenkamp E.T., Wingfield B.D. (2025) Harnessing exogenous membrane vesicles for studying *Fusarium circinatum* and its biofilm communities.

- Microbial Pathogenesis*, **200**, 107368. <https://doi.org/10.1016/j.micpath.2025.107368>
- Ratsoma F.M., Mokoena N.Z., Santana Q.C., Wingfield B.D., Steenkamp E.T., Motaung T.E. (2024) Characterization of the fusarium circinatum biofilm environmental response role. *Journal of Basic Microbiology*, **64**, e2300536. <https://doi.org/10.1002/jobm.202300536>
- Regente M., Pinedo M., San Clemente H., Ballaré C., Pagnussat G., de la Canal L. (2017) Plant extracellular vesicles are incorporated by a fungal pathogen and inhibit its growth. *Journal of Experimental Botany*, **68**, 5485–5495. <https://doi.org/10.1093/jxb/erx355>
- Richardson D.M., Rejmánek M. (2011) Trees and shrubs as invasive alien species – a global review. *Diversity and Distributions*, **17**(5), 788–809. Portico. <https://doi.org/10.1111/j.1472-4642.2011.00782.x>
- Rutter B.D., Innes R.W. (2017) Extracellular vesicles isolated from the leaf apoplast carry stress-response proteins. *Plant Physiology*, **173**, 728–741. <https://doi.org/10.1104/pp.16.01253>
- Schlemmer T., Lischka R., Wegner L., Koch A., Kogel K.-H., Knipfer T., Reichel M., Schellenberger R. (2022) Extracellular vesicles isolated from dsRNA-sprayed barley plants exhibit no growth inhibition or gene silencing in fusarium graminearum. *Fungal Biology and Biotechnology*, **9**, 14. <https://doi.org/10.4314/wsa.v42i1.15>
- Tanzer M.M., Arst H.N., Skalchunes A.R., Coffin M., Darveaux B.A., Heinsohn H.C., Inamine G., Kays A., Kinzel J.S., Kohl C.T., Loop V., Morrell J.A., Parker D.T., Tkaczyk C., Young C.L., McLaughlin M.M. (2003) Global nutritional profiling for mutant and chemical mode-of-action analysis in filamentous fungi. *Functional and Integrative Genomics*, **3**, 160–170. <https://doi.org/10.1007/s10142-003-0089-3>
- Welsh J.A., Goberdhan D.C., O'Driscoll L., Buzás E.I., Blenkiron C., Bussolati B., Cai H., Di Vizio D., Driedonks T.A., Erdbrügger U., Falcon-Perez J.M. (2024) Minimal information for studies of extracellular vesicles (MISEV2023): From basic to advanced approaches. *Journal of Extracellular Vesicles*, **13**, e12404. <https://doi.org/10.1002/jev2.12404>
- Wu R., Chen B., Jia J., Li Y., Zhang Y., Wang C., Zhou H., Qian H., Xu W., Wu S., Zhang Y., Chen J. (2024) Relationship between protein, microRNA expression in extracellular vesicles and rice seed vigor. *International Journal of Molecular Sciences*, **25**, 10504. <https://doi.org/10.3390/ijms251910504>
- Wu Y.X., von Tiedemann A. (2002) Impact of fungicides on active oxygen species and antioxidant enzymes in spring barley (*Hordeum vulgare* L.) exposed to ozone. *Environmental Pollution*, **116**, 37–47. [https://doi.org/10.1016/S0269-7491\(01\)00174-9](https://doi.org/10.1016/S0269-7491(01)00174-9)
- Zhang Z., Yu Y., Zhu G., He S., Zhang Z., Yang T., Zhang L., Tian Y., Zhang S., Chen X., Xu X., Hu X. (2022) The emerging role of plant-derived exosomes-like nanoparticles in immune regulation and periodontitis treatment. *Frontiers in Immunology*, **13**, 896745. <https://doi.org/10.3389/fimmu.2022.896745>